

Investigation of constraints on few-neutron forces in neutron matter by empirical information on the neutron skin of ^{48}Ca and ^{208}Pb

Francesca Sammarruca

Physics Department, University of Idaho, Moscow, ID 83844-0903, U.S.A.

(Dated: November 8, 2016)

The neutron matter equation of state is calculated from two-neutron forces up to fifth order of the chiral expansion and the order-by-order convergence of the predictions is investigated. Based on these equations of state, the binding energies and the neutron and proton density distributions in ^{208}Pb and ^{48}Ca are derived, with particular attention to the neutron skins, the focal point of this paper. Anticipating future experiments which will provide reliable information on the weak charge density in nuclei, the theoretical uncertainties and the possibility of constraining the size of few-neutron forces in neutron matter are discussed.

I. INTRODUCTION

Chiral effective field theory (EFT) has become established as a model-independent approach to construct nuclear two- and many-body forces in a systematic and internally consistent manner [1, 2]. Nucleon-nucleon (NN) potentials have been developed from next-to-leading order (NLO, second order) to N^3LO (fourth order) [3–7], with the latter reproducing NN data at the high precision level. More recently, NN chiral potentials at N^4LO have become available [8, 9].

Consistent application of these potentials in few- and many-body systems requires inclusion of all few- and many-nucleon forces which appear at the given order of chiral EFT, a task of greater and greater complexity with increasing order. In fact, even today, all two-, three-, and four-nucleon forces of order greater than three have not yet been applied in an $A > 3$ system, although several *ab initio* calculations of nuclei and nuclear matter based on chiral EFT have been reported. A fairly extensive, although likely not exhaustive list is given in Refs. [10–29]. Predictions in neutron matter from chiral EFT interactions can be found in Ref. [30].

On the other hand, thanks to recent progress in the development of chiral NN forces [8, 9], internally consistent calculations can be conducted in the many-body system with two-nucleon forces (2NFs) up to fifth order. Although the predictions thus obtained are incomplete, they can provide valuable information on what is missing. Observing the order-by-order convergence of such 2NF based calculations, one can pin down the effect of 3NFs with uncertainty quantification. Together with reliable empirical information on the observables under consideration, the size of the missing 3NFs can be constrained.

Neutron-rich systems are especially interesting and are receiving considerable attention. Neutron-rich nuclei are intriguing for many reasons, ranging from the mechanism that controls the formation of the neutron skin to remarkable correlations with the properties of compact stars. On the other hand, the properties of these nuclei are, in general, poorly constrained. However, the electroweak program at the Jefferson Laboratory promises to deliver accurate measurements of the neutron skin in ^{208}Pb and, potentially, ^{48}Ca . Note that, for the latter nucleus, *ab initio* calculations are now possible [31].

The arguments stated above motivate the present work. It is the purpose of this paper to explore to which extent one can estimate the size of three-neutron forces in neutron matter using empirical constraints. After a description of the novel aspects of this work (Sec. II A) and a brief review of previously developed formalism (Sec. II B), order-by-order results are shown for nuclear properties in ^{208}Pb and ^{48}Ca (Sec. III). For that purpose, microscopic equations of state (EoS) of neutron matter with 2NFs up to 5th order of chiral EFT are first calculated. The theoretical uncertainties arising from diverse sources are discussed and available constraints on the skins of ^{208}Pb and ^{48}Ca are examined to explore the likelihood that future, more stringent constraints would allow to estimate the size of few-neutron forces in neutron matter. Section IV concludes the paper.

II. NUCLEAR PROPERTIES FROM TWO-NUCLEON FORCES UP TO 5TH ORDER

A. The nucleon-nucleon force in neutron matter at N^4LO

The neutron matter EoSs used as input are obtained as in Ref. [32] up to fourth order, but without 3NFs. An important novel aspect here is the extension of the 2NF to fifth order of chiral EFT. The NN interaction employed is the one at N^4LO whose predictions for peripheral partial waves were shown in Ref. [8]. The potential includes one- and two-loop two-pion exchanges and two-loop three-pion exchanges as required at this order, see Fig. 1.

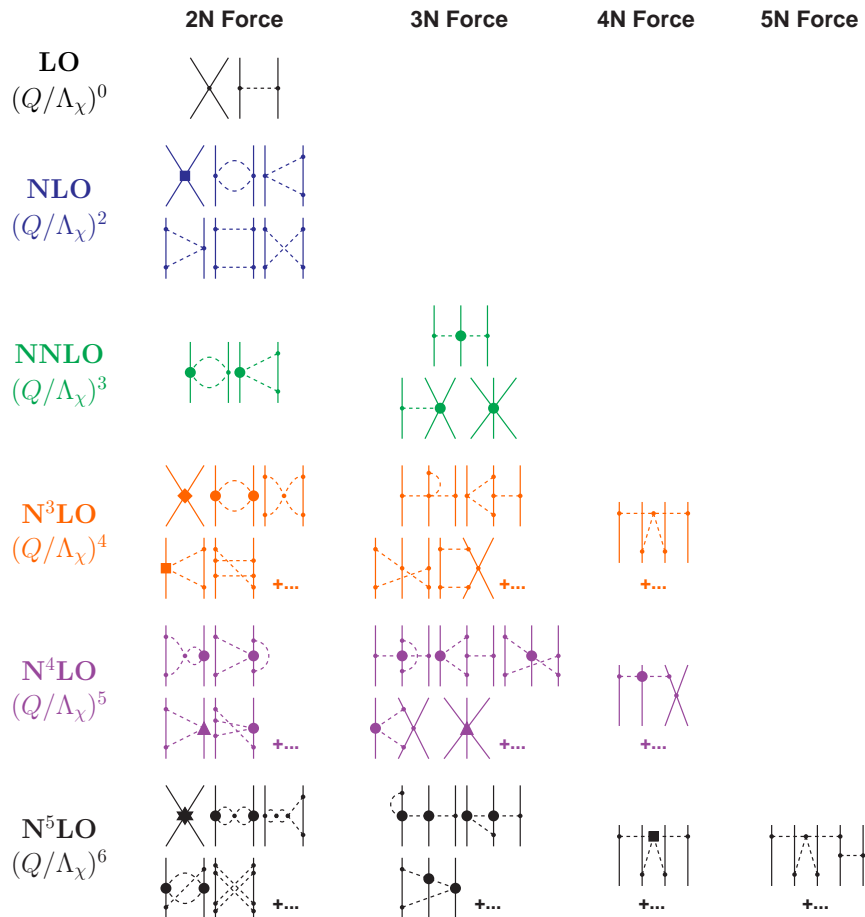


FIG. 1: (Color online) Diagrams of two- and few-nucleon forces appearing at increasing orders of chiral perturbation theory.

Although at $N^2\text{LO}$ the main features of the nuclear force can be described reasonably well, it is well known that one must go to the next order to achieve high precision. However, at $N^3\text{LO}$ (as at $N^2\text{LO}$), the chiral 2π exchange is still too attractive. It is shown in Ref. [8] that the 2π exchange at $N^4\text{LO}$ is mostly repulsive, which allows an improved description of the F and G partial waves. The overall contribution from the 3π exchange is found to be of moderate size, suggesting convergence with regard to the number of exchanged pions. The hierarchy of nuclear forces as they emerge at each order of chiral EFT is displayed in Fig. 1.

The neutron matter EoS is calculated within the particle-particle ladder approximation, order by order from NLO to $N^4\text{LO}$ using 2NFs only. The EoS are displayed in Fig. 2. (Note that the leading order (LO) is not included because it is an extremely poor representation of the nuclear force and thus would not add much to the discussion, even in the context of order-by-order convergence.) The order-by-order pattern shows a clear signature of convergence: The fifth order correction is substantially smaller than the fourth order one.

B. Brief review of additional tools

To facilitate the understanding of the results, this section provides a very brief review of previously developed tools. Nuclear properties are obtained as described in Ref. [33]. Namely, inspired by a liquid droplet model, the energy of a

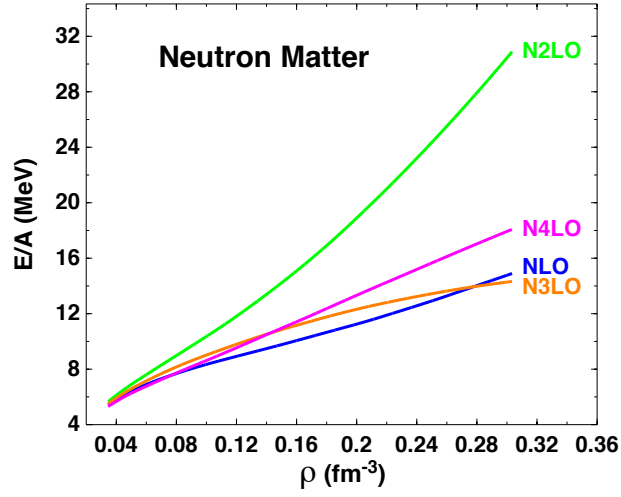


FIG. 2: (Color online) Energy per neutron as a function of neutron matter density ρ obtained with chiral 2NFs at the indicated orders of EFT.

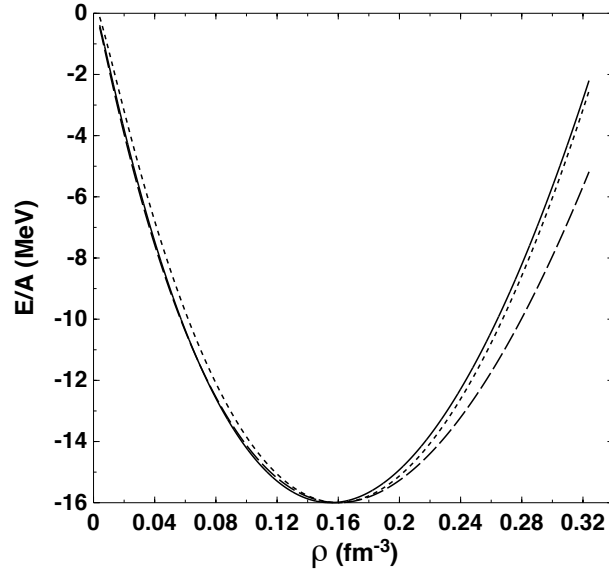


FIG. 3: Phenomenological equations of state for symmetric nuclear matter. Solid: From Ref. [35]; Dashed: From Ref. [36], lower incompressibility; Dotted: From Ref. [36], higher incompressibility. See text for more details.

nucleus is written in terms of a volume, a surface, and a Coulomb term as

$$E(Z, A) = \int d^3r e(\rho, \alpha)\rho(r) + \int d^3r f_0 |\nabla\rho|^2 + \frac{e^2}{4\pi\epsilon_0} (4\pi)^2 \int_0^\infty dr' r' \rho_p(r') \int_0^{r'} dr r^2 \rho_p(r). \quad (1)$$

In the above equation, ρ is the isoscalar density, given by $\rho_n + \rho_p$, α is the neutron asymmetry parameter, $\alpha = \rho_I/\rho$, where the isovector density ρ_I is given by $(\rho_n - \rho_p)$. $e(\rho, \alpha)$ is the energy per particle in isospin-asymmetric nuclear

matter, written as

$$e(\rho, \alpha) = e(\rho, 0) + e_{sym}(\rho)\alpha^2, \quad (2)$$

with $e_{sym}(\rho)$ the symmetry energy. The density functions for protons and neutrons are obtained by minimizing the value of the energy, Eq. (1), with respect to the parameters of Thomas-Fermi distributions,

$$\rho_i(r) = \frac{\rho_0}{1 + e^{(r-a_i)/c_i}}, \quad (3)$$

with $i = n, p$. The radius and the diffuseness, a_i and c_i , respectively, are extracted by minimization of the energy while ρ_0 is obtained by normalizing the proton(neutron) distribution to $Z(N)$. The neutron skin, which is the object of this investigation, is defined as

$$S = R_n - R_p, \quad (4)$$

where R_n and R_p are the *r.m.s.* radii of the neutron and proton density distributions,

$$R_i = \left(\frac{4\pi}{T} \int_0^\infty \rho_i(r) r^4 dr \right)^{1/2}, \quad (5)$$

where $T = N$ or Z . This method has the advantage of allowing for a very direct connection between the EoS and the properties of finite nuclei. It was used in Ref. [33] in conjunction with relativistic meson-theoretic potentials and found to yield realistic predictions for binding energies and charge radii. The constant f_0 in the surface term is typically obtained from fits to β -stable nuclei and found to be about 60-70 MeV fm⁵ [34]. How this uncertainty impacts the corresponding predictions will be discussed below.

The isospin-symmetric part of the EoS in Eq. (2) is taken from phenomenology [35] to maintain the focus on the microscopic neutron matter predictions. The EoS employed here for symmetric matter was obtained from empirically determined values of characteristic constants in homogeneous matter at saturation and subsaturation [35], with isoscalar quantities (and also isovector ones) found to be very well constrained. At the low densities probed by the neutron skin, one might expect that equations of state constructed to reproduce closely empirical properties will not be appreciably different from one another, as is confirmed in Fig. 3. Nevertheless, to estimate the uncertainty associated with different phenomenological parametrizations of the symmetric matter EoS, the phenomenological EoS from Ref. [36], designed to describe both isospin symmetric and asymmetric nuclear matter, will be used in addition. For symmetric nuclear matter, it is given as

$$e(\rho, 0) = \frac{3\hbar^2}{10m} \left(\frac{3\pi^2}{2} \rho \right)^{2/3} + \frac{\alpha}{2} \frac{\rho}{\rho_0} + \frac{\beta}{\sigma + 1} \left(\frac{\rho}{\rho_0} \right)^\sigma, \quad (6)$$

where $\rho_0 = 0.16 \text{ fm}^{-3}$, the energy at saturation is very close to -16 MeV, and α , β , and σ are expressed in terms of the incompressibility K_0 [36] whose commonly accepted value is 240 ± 20 MeV. In Fig. 3, we show the equation of state from Ref. [35] (solid), whose parameters are fitted to the central values of the constraints (e. g. $K_0=240$ MeV), in comparison to the one from Ref. [36] with parameters corresponding to $K_0=(240-20)$ MeV (dashed) or $K_0=(240+20)$ MeV (dotted). The predictions shown by the dotted curve, which appear to differ more noticeably from the solid curve at subsaturation to saturation densities, will be used here to estimate the uncertainty arising from the choice of the phenomenological EoS. In fact, several tests confirmed that the larger differences between the solid and the dashed curves at suprasaturation densities are essentially insignificant for the neutron skin investigations performed here. Note, further, that I am not considering a family of *theoretical* EoS for symmetric matter, since I wish to keep out of this investigation any model dependence which may arise from those.

III. RESULTS

As a first look into order-by-order convergence, I begin this section by showing, cf. Fig. 4, the two-parameter Fermi functions obtained for neutron and proton densities from NLO to N⁴LO. Obviously, order-by-order differences cannot be discerned on the scale of the figure, with the exception of the neutron densities. The green curve (lower curve) reflects the stronger repulsion (hence, lower central densities) of the EoS at N²LO, cf. Fig. 2. The predictions in Fig. 4 are obtained with $\Lambda=450$ MeV, but order-by-order differences remain small when varying the scale, as will be discussed below.

Next, I will focus on the binding energy per nucleon, the charge radius, the point proton and neutron radii, and the neutron skin for ^{48}Ca and ^{208}Pb . I will consider truncation error, sensitivity to cutoff variations, as well as uncertainties associated with the density functional including the choice of the phenomenological EoS.

With regard to the cutoff parameter, which appears in the regulator function

$$f(p', p) = \exp[-(p'/\Lambda)^{2n} - (p/\Lambda)^{2n}], \quad (7)$$

values between 450 and about 600 MeV will be considered, with 550 MeV being the largest available at N⁴LO. Note that these values are below the breakdown scale of chiral EFT [37]. Other analytical expressions are possible for the regulator function [37]. It will be interesting to include these potentials when they become available to the community at large. Furthermore, coordinate-space potentials have been developed up to N²LO for the 2π -exchange contributions and up to N³LO for the contact terms [38]. Therefore, a consistent study at N³LO and beyond, as the one undertaken here, would not be possible with the potentials from Ref. [38].

The results for ^{48}Ca , using the f_0 parameter [cf. Eq. (1)] on the lower side, are shown in Table I. One can see that these nuclear properties show good convergence tendency at N⁴LO. Similar comments apply to Table II, where the predictions differ from those in Table I only in the larger value of f_0 , which introduces more repulsion in the liquid droplet model. Binding energy values are smaller by a few percent and the r.m.s. radii remain very close to those in Table I. Once again, all properties show a clear signature of convergence towards N⁴LO. The results for ^{208}Pb , which are given in Table III and Table IV, show trends very similar to those observed in ^{48}Ca .

In the uncertainty analysis which follows, the results at N³LO will be taken as the “final” predictions, since the truncation error at this order can be reliably estimated from the knowledge of the predictions at N⁴LO. For ^{48}Ca at N³LO, using the smaller value of f_0 (cf. Table I) and averaging the results for the different cutoffs yields $S = 0.148^{+0.002}_{-0.003}$ fm, whereas a similar average for the larger value of f_0 (cf. Table II) gives $S = 0.162^{+0.003}_{-0.003}$ fm.

At N³LO, the truncation error is given by the difference between the predictions at N³LO and those at N⁴LO. Or, in other words: The N⁴LO correction is the N³LO uncertainty. Applying this reasoning, next I take the difference between cutoff-averaged predictions at N³LO and N⁴LO, respectively, and determine the truncation error to be about 0.001 fm, showing that the results are very well converged with respect to the chiral expansion of the two-nucleon force.

Further, to account for the uncertainty arising from the parameter f_0 in the droplet model, the central values given above are averaged, which yields $\bar{S} = 0.155 \pm 0.007$ fm.

The same steps are then repeated using another phenomenological EoS for symmetric matter (see discussion above, at the end of Sect. II B). Using the smaller value of f_0 and averaging the results for the different cutoffs, I obtain $S = 0.155^{+0.002}_{-0.003}$ fm, whereas a similar average for the larger value of f_0 gives $S = 0.169^{+0.0024}_{-0.003}$ fm. The truncation error is again very small (about 0.001 fm). Averaging the central values as before yields $\bar{S} = 0.162 \pm 0.007$ fm.

Finally, combining the results obtained with two phenomenological EoS and calculating the total error in quadrature, the prediction based on chiral 2NFs at N³LO is found to be:

$$\bar{S}_{2NF}(^{48}\text{Ca}) = (0.159 \pm 0.009) \text{ fm} . \quad (8)$$

An identical analysis for ^{208}Pb yields

$$\bar{S}_{2NF}(^{208}\text{Pb}) = (0.14 \pm 0.01) \text{ fm} . \quad (9)$$

The question to be addressed next is whether one can constrain the effect from few-neutron forces in neutron matter using these well-converged results based on 2NFs only and empirical information. Some comments are in place here concerning the nature of the contributions one may potentially constrain. In principle, four- and higher-body forces are included in the missing terms. However, it is reasonable to expect that by far the largest contribution would be from 3NFs. In fact, chiral perturbation theory offers a justification for why higher-body forces should be smaller, since they appear at higher order in the expansion. An investigation aimed at constraining 3NFs exploiting chiral 2NFs can be found in Ref. [39].

Accurate measurements of the neutron skin of ^{208}Pb from PREX experiments [40] (and, potentially, C-REX experiments for ^{48}Ca [41]), are expected but not yet available. Thus, I will start from current information and project a near-future scenario when accurate measurements of neutron radii become available from parity-violating electron scattering experiments.

Table V displays some representative empirical results for the neutron skin thickness of ^{48}Ca and ^{208}Pb extracted by a variety of methods (see corresponding citations). Reference [42] makes use of pionic probes and total π^+ reaction cross sections between 0.7 and 2 GeV/c. The first two values for calcium displayed in Table V are obtained with pionic atoms adopting two different versions of the neutron density [43]. The last entry for calcium was obtained from analyses of π^+ and π^- scattering across the (3,3) resonance [44]. The same comment applies to the first two table

Order	Cutoff(MeV)	B/A (MeV)	r_{ch} (fm)	r_p (fm)	r_n (fm)	S (fm)
NLO	450	8.735	3.620	3.517	3.655	0.138
NLO	500	8.734	3.620	3.517	3.656	0.138
NLO	600	8.735	3.621	3.518	3.658	0.140
N ² LO	450	8.693	3.613	3.510	3.672	0.162
N ² LO	500	8.690	3.613	3.510	3.674	0.164
N ² LO	600	8.686	3.612	3.509	3.675	0.166
N ³ LO	450	8.723	3.618	3.515	3.660	0.145
N ³ LO	500	8.715	3.617	3.514	3.663	0.149
N ³ LO	600	8.714	3.616	3.513	3.663	0.150
N ⁴ LO	450	8.728	3.618	3.515	3.661	0.146
N ⁴ LO	500	8.724	3.617	3.514	3.661	0.147
N ⁴ LO	550	8.722	3.617	3.514	3.662	0.148

TABLE I: Binding energy per nucleon (B/A), charge radius (r_{ch}), proton and neutron point radii (r_p and r_n , respectively), and neutron skin (S) of ^{48}Ca . The predictions are obtained from a microscopic neutron matter equation of state including only two-neutron forces at the specified orders of chiral effective field theory. The value of f_0 in Eq. (1) is 60 MeV fm^5 .

Cutoff (MeV)	Order	B/A (MeV)	r_{ch} (fm)	r_p (fm)	r_n (fm)	S (fm)
NLO	450	8.362	3.659	3.557	3.708	0.152
NLO	500	8.362	3.659	3.557	3.709	0.152
NLO	600	8.363	3.659	3.557	3.711	0.154
N ² LO	450	8.324	3.651	3.549	3.725	0.176
N ² LO	500	8.321	3.651	3.549	3.727	0.178
N ² LO	600	8.318	3.650	3.548	3.728	0.180
N ³ LO	450	8.351	3.656	3.554	3.713	0.159
N ³ LO	500	8.344	3.655	3.553	3.716	0.163
N ³ LO	600	8.343	3.654	3.552	3.717	0.165
N ⁴ LO	450	8.356	3.656	3.554	3.714	0.160
N ⁴ LO	500	8.353	3.655	3.554	3.714	0.161
N ⁴ LO	550	8.350	3.655	3.553	3.715	0.162

TABLE II: Same as Table I, but using $f_0 = 70 \text{ MeV fm}^5$.

Cutoff(MeV)	Order	B/A (MeV)	r_{ch} (fm)	r_p (fm)	r_n (fm)	S (fm)
NLO	450	7.966	5.645	5.580	5.690	0.110
NLO	500	7.963	5.646	5.581	5.693	0.112
NLO	600	7.960	5.649	5.584	5.701	0.117
N ² LO	450	7.862	5.643	5.577	5.730	0.154
N ² LO	500	7.853	5.643	5.578	5.735	0.158
N ² LO	600	7.844	5.644	5.578	5.740	0.162
N ³ LO	450	7.936	5.642	5.576	5.699	0.123
N ³ LO	500	7.917	5.643	5.577	5.708	0.130
N ³ LO	600	7.914	5.641	5.575	5.708	0.132
N ⁴ LO	450	7.943	5.645	5.579	5.705	0.125
N ⁴ LO	500	7.937	5.643	5.577	5.703	0.126
N ⁴ LO	550	7.930	5.642	5.576	5.705	0.129

TABLE III: Same as Table I, but for ^{208}Pb .

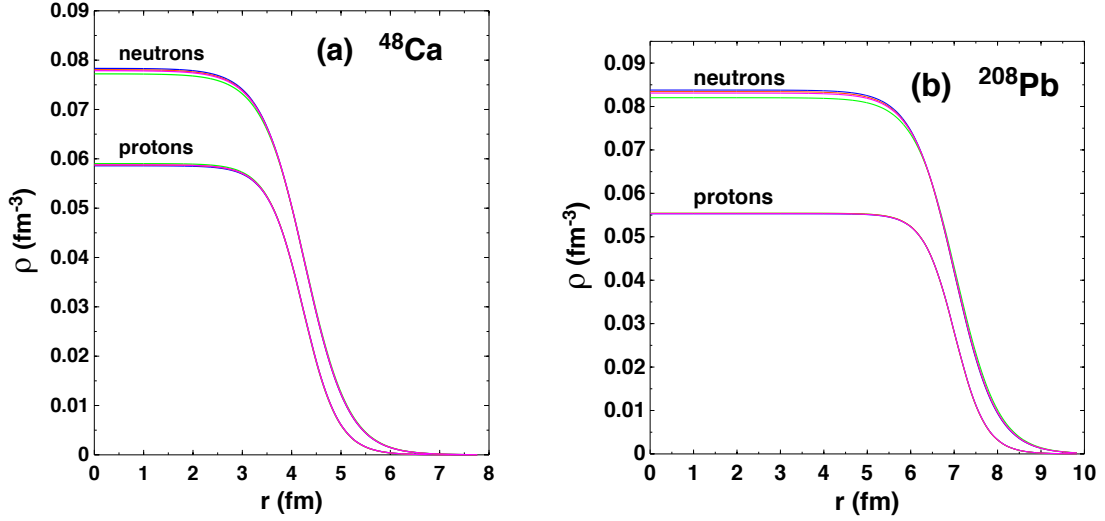


FIG. 4: (Color online) Density distributions for neutrons and protons in (a) ^{48}Ca and (b) ^{208}Pb , for different orders of chiral EFT from NLO to N^4LO . Color code as in Fig. 2. For protons, the various curves cannot be distinguished on the scale of the figures. For neutrons, the lowest (green) curve represents the N^2LO result.

Cutoff(MeV)	Order	$B/A(\text{MeV})$	$r_{ch}(\text{fm})$	$r_p(\text{fm})$	$r_n(\text{fm})$	$S(\text{fm})$
NLO	450	7.741	5.671	5.605	5.729	0.124
NLO	500	7.739	5.672	5.606	5.732	0.125
NLO	600	7.736	5.675	5.609	5.740	0.130
N^2LO	450	7.642	5.667	5.602	5.770	0.169
N^2LO	500	7.634	5.667	5.602	5.775	0.173
N^2LO	600	7.625	5.668	5.603	5.780	0.177
N^3LO	450	7.712	5.667	5.602	5.738	0.137
N^3LO	500	7.694	5.668	5.602	5.747	0.145
N^3LO	600	7.692	5.666	5.601	5.747	0.147
N^4LO	450	7.719	5.670	5.605	5.744	0.139
N^4LO	500	7.714	5.668	5.603	5.743	0.140
N^4LO	550	7.707	5.667	5.602	5.744	0.143

TABLE IV: Same as Table II, but for ^{208}Pb .

entries for lead. The authors of Ref. [45] also make use of pionic atom potentials while varying radial parameters of the neutron distributions. The third entry for lead in Table V is a weighted average of their analysis as well as results from previous models. The last ^{208}Pb entry is extracted from symmetry energy constraints and is consistent with a broad set of skin measurements based on antiprotonic atoms, Pigmy Dipole resonances, electric dipole polarizability, and proton elastic scattering [46].

By averaging the values for ^{48}Ca of Table V and calculating the error in quadrature, one can estimate the current knowledge of the neutron skin in ^{48}Ca as:

$$\bar{S}_{emp}(^{48}\text{Ca}) = (0.13 \pm 0.03) \text{ fm} . \quad (10)$$

The difference between theory and experiment then comes out to be:

$$|\bar{S}_{2NF}(^{48}\text{Ca}) - \bar{S}_{emp}(^{48}\text{Ca})| = (0.03 \pm 0.03) \text{ fm} . \quad (11)$$

Obviously, the difference between the central values from Eqs. (10) and (8) is about the same as the uncertainty and,

Nucleus	S (fm)	Source
^{48}Ca	0.13 ± 0.06	Ref. [42]
	0.16 ± 0.07	Ref. [42]
	0.11 ± 0.04	Ref. [44]
^{208}Pb	0.15 ± 0.08	Ref. [42]
	0.14 ± 0.10	Ref. [42]
	0.18 ± 0.05	Ref. [45]
	0.18 ± 0.05	Ref. [46]

TABLE V: Empirical values for the neutron skin of ^{48}Ca and ^{208}Pb taken from various sources.

therefore, current empirical determinations of the neutron skin of ^{48}Ca cannot pin down the effect of the 3NF on neutron matter.

The situation is similar for ^{208}Pb , where the average of the empirical values shown in Table V results in

$$\bar{S}_{emp}(^{208}\text{Pb}) = (0.16 \pm 0.04) \text{ fm} . \quad (12)$$

Here, the difference between theory and experiment is:

$$|\bar{S}_{2NF}(^{208}\text{Pb}) - \bar{S}_{emp}(^{208}\text{Pb})| = (0.02 \pm 0.04) \text{ fm} , \quad (13)$$

which is smaller than the uncertainty.

To summarize, from the present analysis one may conclude that a measurement of the neutron skin can provide a constraint for the effect of 3NFs on neutron matter if the experimental uncertainty is $\Delta\bar{S}_{emp} < |\bar{S}_{2NF} - \bar{S}_{emp}|$. Based on the above values, one may conclude that future experiments on the neutron skin of ^{208}Pb (or ^{48}Ca) should aim for an uncertainty $\Delta\bar{S}_{emp} < 0.03$ fm to provide a useful constraint on 3NFs in neutron matter.

IV. SUMMARY AND CONCLUSIONS

Predictions which cannot be stated with appropriate theoretical uncertainty are no longer consistent with contemporary standards. With chiral EFT, one can reliably estimate the truncation error at each order of the chiral expansion. Being able to do so is crucial to guide future measurements.

In this work, the neutron matter EoS applying chiral 2NFs up to fifth order has been calculated, thus extending previous predictions. Using as input the microscopic neutron matter EoS from second order to fifth order, the order-by-order convergence pattern of the neutron skin in ^{48}Ca and ^{208}Pb was explored. It turns out that the uncertainty with regard to the chiral expansion of the 2NF up to N⁴LO is 0.001 fm for both nuclei, which reflects an excellent degree of convergence concerning the Hamiltonian. Including (non-local) cutoff variations and the error from the many-body method applied, the overall uncertainty of these predictions comes out to be about 0.01 fm for ^{48}Ca and ^{208}Pb . This small theoretical uncertainty of the 2NF based predictions should, in principle, allow to pin down the effects of the missing 3NFs, if the empirical determination carries a sufficiently small error, which is not the case with present constraints. This analysis finds that the experimental error of neutron skin determinations for these nuclei should be less than 0.03 fm to be effective in constraining missing contributions from few-nucleon forces. These findings can be a useful guideline for planners of future PREX/CREX experiments.

Before closing, it is important to remind the reader that this analysis will be broadened in the near future. In particular:

- The uncertainty analysis should be extended to include a full variation of the regulator function, namely both scheme and scale;
- At this time, the EoS of symmetric matter has been kept fixed to an empirical one, in order to maintain the focus on the possibility to constrain three-neutron forces in neutron matter. The information obtained in the present study will be useful when moving on to a similar investigation which employs, instead, fully microscopic EoS of symmetric matter at each chiral order.

Acknowledgments

This work was supported by the U.S. Department of Energy, Office of Science, Office of Basic Energy Sciences, under Award Number DE-FG02-03ER41270.

-
- [1] S. Weinberg, *Physica* **96A**, 327 (1979).
 - [2] S. Weinberg, *Phys. Lett. B* **251**, 288 (1990).
 - [3] E. Marji, A. Canul, Q. MacPherson, R. Winzer, Ch. Zeoli, D.R. Entem, and R. Machleidt, *Phys. Rev. C* **88**, 054002 (2013).
 - [4] D.R. Entem and R. Machleidt, *Phys. Rev. C* **68**, 041001 (2003).
 - [5] R. Machleidt and D.R. Entem, *Physics Report* **503**, 1 (2011).
 - [6] E. Epelbaum, W. Glöckle, and U.-G. Meissner, *Nucl. Phys. A* **747**, 362 (2005).
 - [7] E. Epelbaum, H.-W. Hammer, and U.-G. Meissner, *Rev. Mod. Phys.* **81**, 1773 (2009).
 - [8] D.R. Entem, N. Kaiser, R. Machleidt, and Y. Nosyk, *Phys. Rev. C* **91**, 014002 (2015).
 - [9] E. Epelbaum, H. Krebs, and U.-G. Meissner, *Phys. Rev. Lett.* **115**, 122301 (2015).
 - [10] B.R. Barrett, P. Navrátil, and J.P. Vary, *Prog. Part. Nucl. Phys.* **69**, 131 (2013).
 - [11] S. Binder, J.Langhammer, A. Calci, and R. Roth, *Phys. Lett. B* **736**, 119 (2014).
 - [12] S. Binder, J.Langhammer, A. Calci, P. Navrátil, and R. Roth, *Phys. Rev. C* **87**, 021303 (2013).
 - [13] G. Hagen, T. Papenbrock, D.J. Dean, and M. Hjorth-Jensen, *Phys. Rev. Lett.* **101**, 092502 (2008).
 - [14] H. Hergert, S. Bogner, T. Morris, A. Schwenk, and K. Tsukiyama, *Phys. Rep.* **621**, 165 (2016).
 - [15] S.R. Stroberg, H. Hergert, J.D. Holt, S.K. Bogner, and A. Schwenk, *Phys. Rev. C* **93**, 051301 (2016).
 - [16] J. Simonis, K. Hebeler, J.D. Holt, J. Menendez, and A. Schwenk, *Phys. Rev. C* **93**, 011302 (2016).
 - [17] K. Hebeler, J. Holt, J. Menendez, and A. Schwenk, *Annual Review of Nuclear and Particle Science* **65**, 457 (2015).
 - [18] A. Ekström *et al.*, *Phys. Rev. C* **91**, 051301 (2015).
 - [19] T.A. Lähde, E. Epelbaum, H. Krebs, D. Lee, U.-G. Meissner, and G. Rupak, *Phys. Lett. B* **732**, 110 (2014).
 - [20] L. Coraggio, J.W. Holt, N. Itaco, R. Machleidt, L.E. Marcucci, and F. Sammarruca, *Phys. Rev. C* **89**, 044321 (2014).
 - [21] A. Cipollone, C. Barbieri, and P. Navrátil, *Phys. Rev. Lett.* **111**, 062501 (2013).
 - [22] V. Somá, A. Cipollone, C. Barbieri, P. Navrátil, and T. Duguet, *Phys. Rev. C* **89**, 061301 (2014).
 - [23] A. Cipollone, C. Barbieri, and P. Navrátil, *Phys. Rev. C* **92**, 014306 (2015).
 - [24] A. Carbone, A. Rios, and A. Polls, *Phys. Rev. C* **88**, 044302 (2013).
 - [25] H. Hergert, S. Binder, A. Calci, J. Langhammer, and R. Roth, *Phys. Rev. Lett.* **110**, 242501 (2013).
 - [26] S. Fiorilla, N. Kaiser, and W. Weise, *Nucl. Phys. A* **880**, 65 (2012).
 - [27] S. Bogner, R. Furnstahl, H. Hergert, M. Kortelainen, P. Maris, *et al.*, *Phys. Rev. C* **84**, 044306 (2011).
 - [28] P. Navrátil, R. Roth, and S. Quaglioni, *Phys. Rev. C* **82**, 034609 (2010).
 - [29] V. Lapoux, V. Somá, C. Barbieri, H. Hergert, J.D. Holt, and S.R. Stroberg, *Phys. Rev. Lett.* **117**, 05250 (2016).
 - [30] T. Krüger, I. Tews, K. Hebeler, and A. Schwenk, *Phys. Rev. C* **88**, 025802 (2013).
 - [31] G. Hagen *et al.*, *Nature Physics* **12**, 186 (2016).
 - [32] F. Sammarruca, L. Coraggio, J.W. Holt, N. Itaco, R. Machleidt, and L.E. Marcucci, *Phys. Rev. C* **91**, 054311 (2015).
 - [33] D. Alonso and F. Sammarruca, *Phys. Rev. C* **68**, 054305 (2003).
 - [34] K. Oyamatsu, Kei Iida, and Hiroyuki Koura, *Phys. Rev. C* **82**, 027301 (2010).
 - [35] N. Alam, B.K. Agrawal, J.N. De, S.K. Samaddar, G. Coló, *Phys. Rev. C* **90**, 054317 (2014).
 - [36] LieWen Chen, arXiv:0910.0086 [nucl-th]; *Sci. China* **G52**, 1494 (2009).
 - [37] E. Epelbaum, H. Krebs, and U.-G. Meissner, *Eur. Phys. J.* **A51**, 53 (2015).
 - [38] M. Piarulli, L. Giralda, R. Schiavilla, R. Navarro Perez, J.E. Amaro, and E. Ruiz Ariola, *Phys. Rev. C* **91**, 024003 (2015); M. Piarulli *et al.*, arXiv:1606.06335 [nucl-th].
 - [39] S. Binder, A. Ekström, T. Papenbrock, K.A. Wendt, *Phys. Rev. C* **93**, 044002 (2016).
 - [40] S. Abrahamyan *et al.* (PREX Collaboration), *Phys. Rev. Lett.* **108**, 112502 (2012).
 - [41] J. Mamei *et al.*, <http://hallaweb.jlab.org/parity/prex/c-rex/c-rex.pdf>.
 - [42] E. Friedman, *Nucl. Phys. A* **896**, 46 (2012); and references therein.
 - [43] A. Trzcińska, J. Jastrzebski, P. Lubinski, F.J. Hartmann, R. Schmidt, T. von Egidy, and B. Klos, *Phys. Rev. Lett.* **87**, 082501 (2001).
 - [44] W.R. Gibbs and J.-P. Dedonder, *Phys. Rev. C* **46**, 1825 (1992).
 - [45] C. García-Recio, J. Nieves, E. Oset, *Nucl. Phys. A* **547**, 473 (1992).
 - [46] M.B. Tsang, J.R. Stone, F. Camera, P. Danielewicz, S. Gandolfi, K. Hebeler, C.J. Horowitz, J. Lee, W.G. Lynch, Z. Kohley, R. Lemmon, P. Moller, T. Murakami, S. Riordan, X. Roca-Maza, F. Sammarruca, A.W. Steiner, I. Vidana, and S.J. Yennello, *Phys. Rev. C* **86**, 015803 (2012); and references therein.